IOP Publishing Journal of Physics B: Atomic, Molecular and Optical Physics
J. Phys. B: At. Mol. Opt. Phys. **53** (2020) 085602 (8pp) https://doi.org/10.1088/1361-6455/ab728c

Ionization of helium by an ultrashort extreme-ultraviolet laser pulse

J Venzke[1], **A Jaroń-Becker** and **A Becker**

JILA and Department of Physics, University of Colorado, Boulder, CO 80309-0440, United States of America

E-mail: joel.venzke@colorado.edu

Received 11 October 2019, revised 14 January 2020
Accepted for publication 3 February 2020
Published 1 April 2020

Abstract

We theoretically study photoelectron angular distributions and related anisotropy parameters for the competition of one- and two-photon ionization of He in an ultrashort extreme-ultraviolet laser pulse, using numerical results from the time-dependent Schrödinger equation. We explore the transition between the two processes for variation of the pulse duration, peak intensity, and central frequency or photoelectron energy. In the results obtained for fixed pulse parameters the transition and interference between the processes can be observed in the even (β_2, β_4) and odd (β_1, β_3) parameters, respectively, while the onset of the impact of three-photon ionization is observed via β_5 at high peak intensities. Finally, we show that the transition can be observed via the even anisotropy parameters in pulses without carrier-to-envelope stabilization as well as in free-electron laser pulses with fluctuating pulse shape.

Keywords: ultrashort laser pulses, EUV laser pulses, ionization

(Some figures may appear in colour only in the online journal)

1. Introduction

The production of extreme-ultraviolet (EUV) pulses using high harmonic generation (HHG) and free-electron lasers (FELs) has led to a resurgence of multiphoton ionization studies in the perturbative intensity regime recently [1–18]. Along with experimental techniques, such as velocity map imaging [19, 20] or cold target recoil ion momentum spectroscopy [21], the detection of angle-resolved emission of the photoelectron following few-photon ionization of atomic and molecular targets has become possible [11]. Photoelectron angular distributions (PADs) are determined by the amplitudes and phases of the partial waves of all pathways contributing to the emission at a given energy into a given solid angle. PADs and related anisotropy parameters are therefore useful observables to obtain quantitative insights in the relative strength of the different pathways and their competition. This has been demonstrated in the past for the competition between resonant and non-resonant two-photon ionization pathways [9–11] and for one- and two-photon ionization channels [13, 14, 17].

Two-photon ionization of atoms, specifically the helium atom, have been studied in theory and experiment in the past, first concerning total ionization yields [1–6, 8] and, more recently, with a focus on PADs [9–11, 17]. It has been shown, that the PADs strongly depend on the pulse duration or, equivalently, the spectral width of the EUV pulses. Initially, theoretical studies by Ishikawa and Ueda revealed that the competition between resonant and non-resonant pathways depends on the pulse width [9, 10]. Changes in the PADs for 1–21 fs pulses at photon energies below the first ionization energy were characterized by the even anisotropy parameters β_2 and β_4. Via these parameters the relative phase between the *s*- and *d*-wave packets for the photoelectron emission can be determined. Related experimental work at the SPring-8 Compact SASE Source test accelerator verified the co-presence of the two pathways [11]. Very recently, Boll *et al* extended these studies, covered a much wider photon energy range and explored the impact of radial and angular electron correlation [17]. They showed that in the low-energy regime a single-active-electron picture is valid while at higher energies in the regime of autoionizing states angular correlations play a major role for the understanding of the PADs.

[1] Author to whom any correspondence should be addressed.

The ongoing quest in shortening pulses at extreme- and deep-ultraviolet wavelengths towards the single-cycle regime in duration are achieved via large spectral widths. Such broadband energy pulses give rise to competition between one- and two-photon (as well as three-photon) ionization processes for emission at a given energy. As mentioned in [17], in helium atom this leads to the additional interference of the *s*- and *d*-wave packets due to two-photon absorption with a *p*-wave packet from single photon absorption. In this work, we study the transition regime between single photon ionization and two-photon absorption. We first show how in this regime the PADs quickly change over a small window of pulse duration, about 1 cycle in full width at half maximum (FWHM). The variation is reflected in the anisotropy parameters β_i ($i = 1$, 2, 3 and 4), which show the transition as well as the interference between the ionization pathways. The dependence on pulse duration, photon energy as well as photoelectron energy is studied. We further consider how variation of pulse parameters, such as the carrier-envelope-phase (CEP), the peak intensity, and the partial coherence of FEL pulses, do impact the anisotropy parameters. Finally, we briefly study at which intensities three-photon ionization, which occurs for these large bandwidth pulses as well, may become observable. In order to accurately account for the different pulse parameters, we have performed simulations based on the time-dependent Schrödinger equation. Since a recent study has shown that for pulses with central photon frequency below the first ionization potential of the helium atom the single active electron (SAE) picture remains valid [17], we have used a SAE potential for our numerical simulations.

2. Methods

2.1. Numerical solution of time-dependent schrödinger equation

We solve the time dependent Schrödinger equation for the interaction of a electron in a spherically symmetric SAE potential with the electric field **E** of a linearly polarized laser pulse (along the $\hat{z}$-direction) in dipole approximation and length gauge (we use Hartree atomic units $e = m_e = \hbar = 1$):

$$i\frac{\partial}{\partial t}\Psi(\mathbf{r}, t) = \left[-\frac{\nabla^2}{2} - \mathbf{E}(t)\cdot\mathbf{z} + V(r)\right]\Psi(\mathbf{r}, t). \quad (1)$$

The wavefunction Ψ is expanded in spherical harmonics up to $l_{max} = 20$ with $m = 0$ due to the symmetry of the problem. The radius is discretized using fourth order finite difference method with a grid spacing of 0.05 a.u. and a maximum radius of 300 a.u. We utilized the exterior complex scaling method on the outer 30 a.u. of the grid. The wavefunction is propagated in time using the Crank–Nicolson method with a time step of 0.01 a.u. In test calculations the numerical code was compared against results from a previously used 2D cylindrical code [22], results from time-dependent perturbation theory in the appropriate intensity and frequency regimes, as well as results reported in the literature [23]. Quantitative agreement was achieved.

In our work we consider ionization of helium atom with pulses at central photon energies below the first ionization potential. In a recent study [17] it has been shown that in this photon energy regime the SAE picture remains valid. We therefore utilize a SAE potential for helium atom

$$V(r) = -\frac{1}{r} - \frac{e^{-2.0329r}}{r} - 0.3953e^{-6.1805r}. \quad (2)$$

Our numerical simulations have been performed for laser pulses with central frequencies at or near to the energy difference between the field-free 1*s* and 2*p* state of the helium atom. In our SAE model of helium the ground state energy is -0.944 a.u., while the 2*p* energy is -0.128 a.u.

To ensure that the electric field integrates to zero [24], we set the vector potential as

$$A(t) = A_0 \exp\left(-\ln(2)\left(\frac{2(t-\tau_0)}{T}\right)^2\right) \times \sin\left(w_A(t-\tau_0) + \phi\right) \quad (3)$$

with $A_0 = \frac{c\sqrt{I_0}}{\omega_A}$, $T = \frac{2\pi N}{\omega_A}$, c is the speed of light, I_0 the peak intensity, N the number of cycles in the pulse, ω_A denotes the central frequency of the vector potential, and ϕ is the carrier-to-envelope phase. The electric field is then obtained as

$$E(t) = -\frac{1}{c}\frac{\partial}{\partial t}A(t). \quad (4)$$

The central frequencies of the spectral distributions of the vector potential, ω_A, and the electric field, ω_E, can differ significantly for an ultrashort laser pulse [25]. In the presentation of the results below we state the physically relevant central frequency ω_E, in the simulations ω_A is determined such that ω_E matches the reported central frequency [25].

2.2. Anisotropy parameters

As result of our *ab initio* numerical calculations we obtain the wavefunction at the end of the interaction with the laser pulse. Via projection on continuum states we can then determine the ionization probability as well as photoelectron energy and angular distributions. If more than one pathway here, e.g. one- and two-photon ionization, contributes to the emission of the photoelectron at a given energy in a given direction, our numerical simulations do not allow for the separate the respective probabilities for each channel easily. This is in contrast to calculations based on perturbation theory, in which the amplitude for each pathway is evaluated and can be analyzed separately. In order to analyze the dominant pathways for photoemission as functions of intensity, photoelectron energy and pulse duration, we therefore determine anisotropy parameters (β-parameters), which provide quantitative insights in the different pathways involved as well as the interference between them [13, 14, 17].

It has been shown [26] that the PAD for an isotropic target is given by:

$$P(E, \theta) = \frac{\sigma(E)}{4\pi}\left[1 + \sum_{j=1}^{n}\beta_j(E)P_j(\cos(\theta))\right] \quad (5)$$

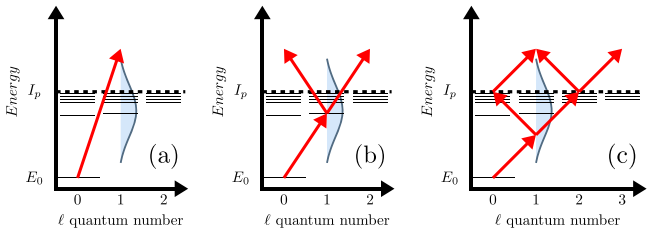

Figure 1. Schematic representation of one- (a), two- (b), and three-photon (c) ionization in an ultrashort pulse. The Gaussian distribution shows the spectral width of the ultrashort pulse centered about the energy of the 2*p*-state. The red arrows represent the photon absorption pathways, and the black lines depict some of the resonant structure of the helium atom.

where θ is the angle of electron emission with respect to the polarization direction of the laser field, while $\sigma(E)$ is the ionization probability at E and P_j are the Legendre polynomials. The anisotropy parameters β_j depend on the amplitudes of the different pathways leading to emission of the photoelectron (for explicit expressions, see [13]). For combinations of one- and two-photon ionization processes, that will be the focus of this work, contributions from the first four β_j-parameters are expected. The contributions related to the odd polynomials indicate interference between partial waves resulting from one- and two-photon absorption. We also note that the impact of three-photon ionization, that we will briefly consider below, is expected to show up in the anisotropy parameter β_5 and higher order parameters.

We have determined the anisotropy parameters in our calculations using equation (5) as follows. At the end of the simulations of the time-dependent Schrödinger equation we obtained the PAD at a given momentum k by projecting the wavefunction onto the field-free continuum states on the numerical grid. The numerically obtained PAD has been then projected onto the jth Legendre polynomial P_j ($j = 1, \ldots, 5$) and the results have been normalized using the total ionization probability σ.

3. Results and discussion

Following a general discussion of the processes involved in section 3.1, we present PADs and related anisotropy parameters for pulses having a Gaussian envelope. The results are analyzed, in view of a competition between one- and two-photon ionization, as a function of pulse duration, central frequency and peak intensity in section 3.2. Fluctuations of the CEP, the peak intensity and the partial coherence of FEL pulses are studied in section 3.3.

3.1. Impact of one-, two-, and three-photon processes in ultrashort pulses

To first illustrate the impact of the one-, two- and three-photon ionization pathways on the emission of the photoelectron in ultrashort laser pulses, let us consider an emission induced by a pulse with central frequency ω_0 tuned to the 1*s*–2*p* energy gap. The broad energy spectrum of an ultrashort Gaussian pulse is schematically depicted in the panels of figure 1 centered about the energy of the 2*p*-state. Absorption of two photons by an electron in the ground state at the central frequency ω_0 (see, figure 1(b)) will lead to its emission at energy $E = 2\omega_0 - |E_{1s}|$. If the bandwidth of the pulse is broad enough (i.e. the pulse duration is sufficiently short) ionization of a photoelectron with the same photoelectron energy can occur via absorption of one photon with energy $2\omega_0$ (see, figure 1(a)) or via absorption of three photons with energy $\frac{2}{3}\omega_0$ (see, figure 1(c)). We note that besides the two-photon and three-photon pathways with absorption of photons of equal energies, there exist more such pathways to a final photoelectron energy E for absorption of photons with unequal energy as long as the sum of the photon energies is equal to $2\omega_E$.

The occurrence of the one- and three-photon processes requires a broad spectral bandwidth of the pulse. That means, for long pulses we expect that only the two-photon ionization process is present. If the pulse is shortened to a few optical cycles, both the one- and three-photon channels become effective, since the probability of photon absorption at energies away from the central frequency increases. In the perturbative intensity regime the probability for a n-photon process scales as I^n, where I is the intensity of the pulse. We therefore expect that at a given ultrashort pulse duration at low intensities the one-photon process dominates over the two-photon process in an ultrashort laser pulse. As the intensity increases, first the two-photon process should then become dominant, before at significant high intensities contributions from the three-photon process will become detectable. In the present paper, we mainly study the transition from one- to two-photon processes, while the influence of the three-photon process will be given minor attention.

3.2. One- versus two-photon ionization

In figure 2 we present examples of PADs that show the transition from single photon ionization, illustrated by the *p*-wave character of the distribution (panels (d), (g), (h)), to an emission following two-photon absorption, highlighted by the dominating *d*-wave character in the PAD (panels (b), (c), (f)). The results are obtained for ionization by a laser pulse at a central photon energy $\omega_0 = 22$ eV, which corresponds to the energy difference between the 1*s*- and 2*p*-states in the single-active-electron potential for helium used in the calculations, peak intensity $I_0 = 10^{11}\,\mathrm{W\,cm^{-2}}$ and carrier-to-envelope phase $\phi = 0$. At a given photoelectron energy, the transition occurs for a variation of the pulse duration, e.g. at $E = 2\omega_0 - |E_{1s}| = 0.687$ a.u. from 0.112 to 0.335 fs (middle row). Conversely, for a fixed pulse duration, the transition is seen for increase of the photoelectron energy, e.g. at $\tau = 0.224$ fs from 0.4 to 1.0 a.u. (middle column). In the transition regime the PADs exhibit the interference between the one- and two-photon ionization processes.

Further insights in the transition between the two processes can be found via the cross section $\sigma(E)$ and the first four anisotropy parameters β_i ($i = 1, \ldots, 4$). In figure 3 the results for the cross section are shown as function of peak intensity at fixed photon and photoelectron energies. The

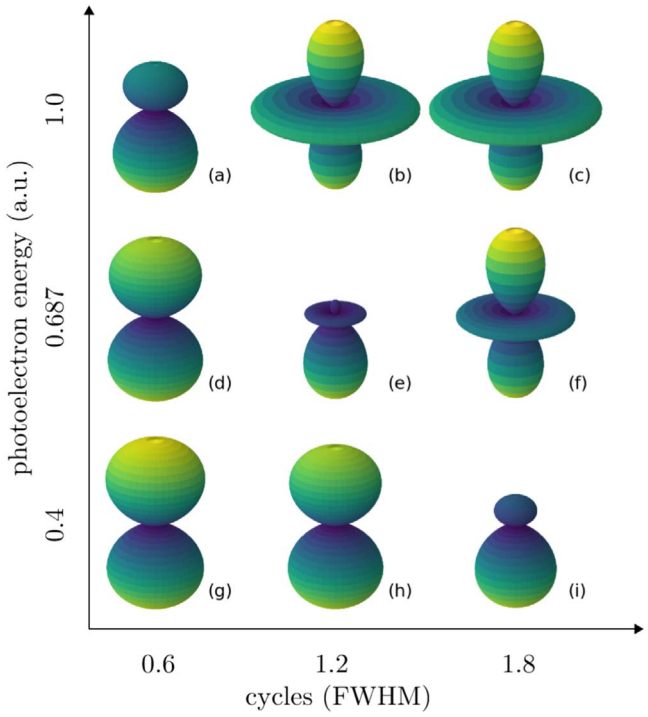

Figure 2. Photoelectron angular distributions for helium atom ionized by laser pulses at central photon energy $\omega_0 = 22.2$ eV, peak intensity $I_0 = 10^{11}$ W cm^{-2}, carrier-to-envelope phase $\phi = 0$ and three different pulse durations: $N = 0.6$ FWFM cycles (0.112 fs, left column), $N = 1.2$ FWHM cycles (0.224 fs, middle column) and $N = 1.8$ FWHM cycles (0.335 fs, right column). Angular distributions are obtained for three values of photoelectron energy $E = 1.45(2\omega_0 - |E_{1s}|) = 1.0$ a.u. (top row), $E = 2\omega_0 - |E_{1s}| = 0.687$ a.u. (middle row), and $E = 0.58(2\omega_0 - |E_{1s}|) = 0.4$ a.u. (bottom row), where E_{1s} is the energy of the $1s$ state in the SAE potential.

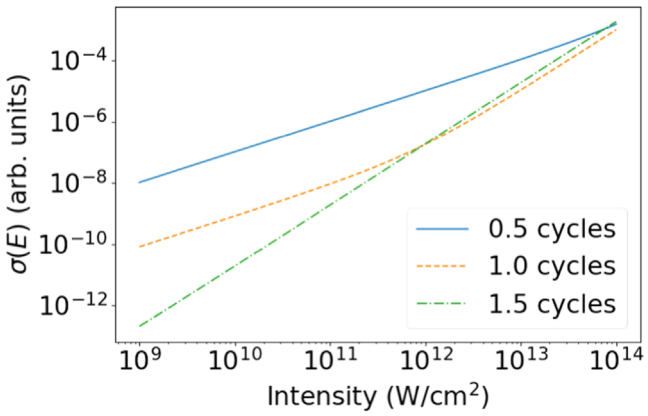

Figure 3. Cross section $\sigma(E)$ as a function of peak intensity for photoelectron emission at energy $E = 2\omega_0 - I_p = 18.7$ eV in 0.5-cycle (one-photon process dominates), 1.0-cycle (transition regime), and 1.5-cycle (two-photon process dominates). Central photon energy $\omega_0 = |E_{2p} - E_{1s}| = 22.2$ eV and carrier-to-envelope phase $\phi = 0$

cross section for a 0.5 cycle pulse has a slope of one corresponding to the dominance of one photon ionization over the whole intensity regime. In contrast, the cross section obtained for the 1.5 cycle pulse is dominated by the two photon process due to the reduced bandwidth of the pulse. In the data for the one-cycle pulse the transition from the one- to the two-photon process is seen to occur near 10^{12} W cm^{-2}.

In figure 4 the results for the β-parameters are shown as function of pulse duration and peak intensity at fixed photon and photoelectron energies. The even β-parameters show the transition from dominant one-photon ionization ($\beta_2 > 0$, $\beta_4 \approx 0$) to dominant two-photon ionization ($\beta_2 \approx 0$, $\beta_4 > 0$), while the odd β-parameters exhibit the regime of interference between the two processes ($\beta_1 < 0$ and $\beta_3 < 0$ for $\phi = 0$). The latter peak where the magnitudes of the two transition amplitudes coincide. At a given peak intensity the interference regime extends over a change of pulse duration of about 0.5 cycles at FWHM. For a fixed pulse duration, the interference regime extends over a variation of peak intensity by a factor of 2–5. The results are therefore rather stable with respect to intensity fluctuations of the pulse. The impact of other potential pulse fluctuations in the experiment on the β-parameters will be discussed in section 3.3.

The transition probabilities of the one- and two-photon processes, σ_1 and σ_2, scale linearly and quadratically with intensity. Assuming that the two-photon ionization process involves predominantly the absorption of photons at equal energies, the peak intensity at maximum interference can be estimated as $I_{infer} \propto D^{(1)}(E) f(\Omega) / (D^{(2)}(E) f^2(\omega))$, where $D^{(i)}(E)$ is the square of the transition dipole moments for the one- and two-photon process, f is the spectral distribution of the pulse and $\Omega = 2\omega = E + |E_{1s}|$. Since $\omega = \omega_0$ for the results in figure 4, $f(\omega) = f(\omega_0) = 1$ and $I_{infer} \propto f(\Omega)$. Thus, we expect that the interference between the two processes requires a larger spectral bandwidth, i.e. shorter pulse duration, the larger the peak intensity of the pulse. The results in figure 4 confirm this expectation.

Next, we consider how the transition between the two pathways depends on the photoelectron energy and the central photon frequency at a given peak intensity $I_0 = 10^{11}$ W cm^{-2} and carrier-to-envelope phase $\phi = 0$. To this end, we show in the figure 5 the anisotropy parameters β_1 (left column) and β_2 (right column) as a function of photoelectron energy and pulse duration for central frequencies below (top row), on (middle row) and above (bottom row) resonance with the $1s - 2p$ transition in the helium single-active-electron potential. We restrict ourselves to β_1 and β_2 since the higher order β-parameters contain equivalent information (see figure 4). Also shown in figure 5 is the photoelectron energy $E = 2\omega_0 - I_p$, corresponding to a two-photon transition at the central frequency ω_0.

The comparison shows that the transition regime depends on the central frequency, since the regime shifts for a given pulse duration to larger photoelectron energies as the central frequencies increases (from bottom to top). At a given central frequency, the pulse duration, at which the transition between the one- and two-photon ionization pathways occurs, increases as the photoelectron energy decreases. Qualitatively, this dependence can be understood using the relation $I_{infer} \propto D^{(1)}(E) f(\Omega) / (D^{(2)}(E) f^2(\omega))$. For photoelectron energies larger than $E = 2\omega_0 - I_p$ (dashed line), both ω and Ω are larger than the central frequency. Consequently, at large photoelectron energies a broader spectral distribution (shorter

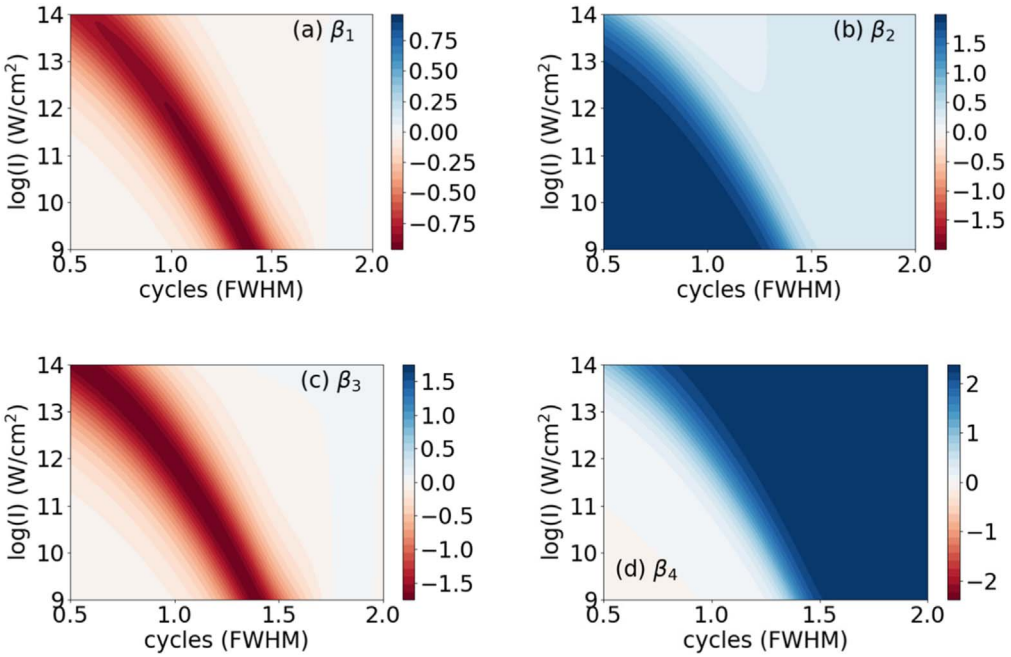

Figure 4. Parameters β_1 (a) to β_4 (d) as function of pulse duration (FWHM) and peak intensity. Central photon energy $\omega_0 = |E_{2p} - E_{1s}| = 22.2$ eV, carrier-to-envelope phase $\phi = 0$ and photoelectron energy $E = 2\omega_0 - I_p = 18.7$ eV.

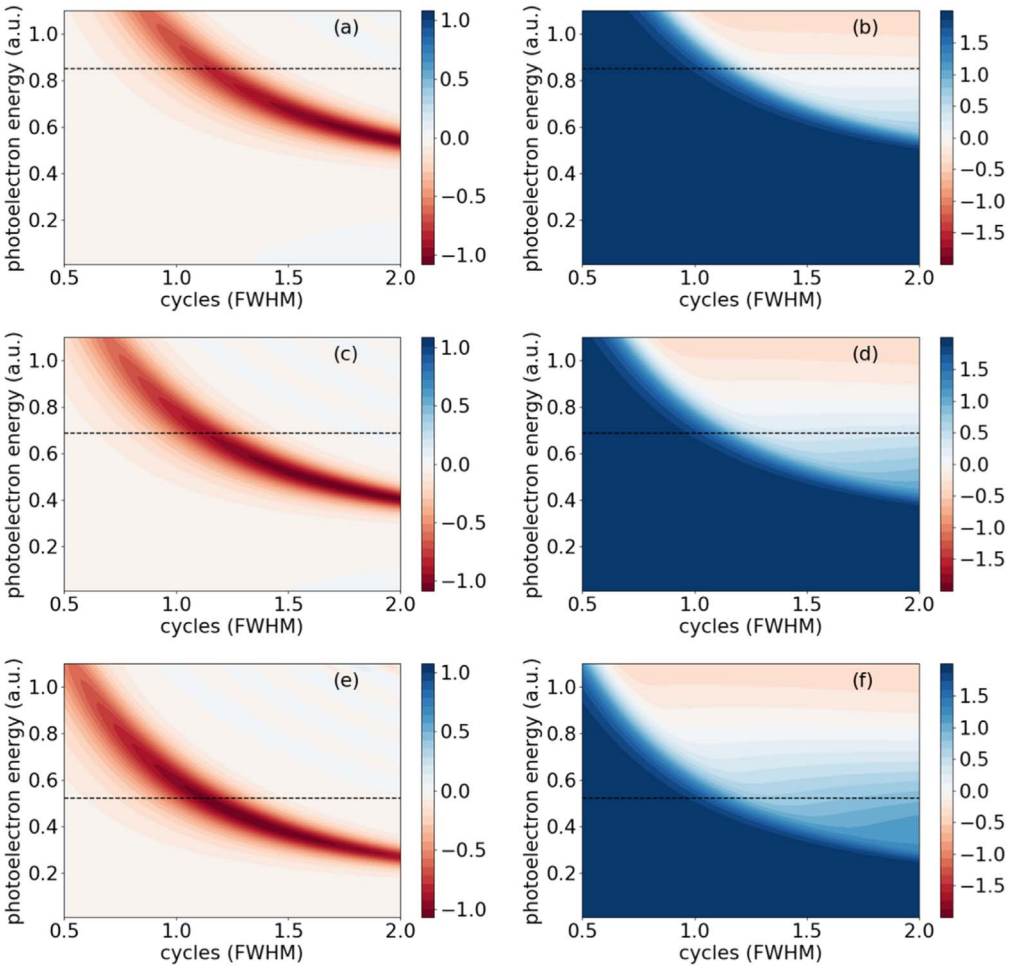

Figure 5. Anisotropy parameters β_1 (left) and β_2 (right) as function of pulse duration and photoelectron energy E for central frequencies $\omega_0 = 1.1|E_{1s} - E_{2p}|$ (top row), $\omega_0 = |E_{1s} - E_{2p}|$ (middle row) and $\omega_0 = 0.9|E_{1s} - E_{2p}|$ (bottom row) at peak intensity of 10^{11} W cm^{-2} and $\phi = 0$. In each panel the dashed line corresponds to $E = 2\omega_0 - I_p$.

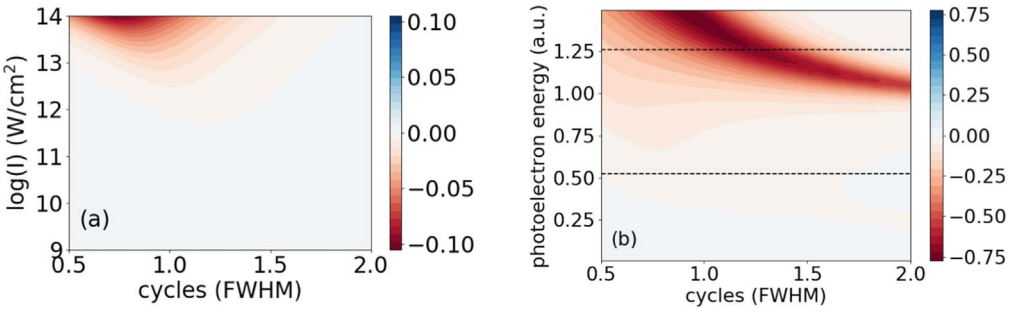

Figure 6. Anisoptropy parameter β_5 (a) as function of pulse duration and peak intensity at central frequency $\omega_0 = |E_{1s} - E_{2p}|$ and photoelectron energy $2\omega_0 - |E_{1s}|$ and (b) as function of pulse duration and photoelectron energy at central frequency $\omega_0 = 0.9|E_{1s} - E_{2p}|$ and peak intensity of 10^{13} W cm^{-2}. The dotted lines correspond to $E = 2\omega_0 - I_p$ and $E = 3\omega_0 - I_p$. The other parameters are as in figures 4 and 5, respectively.

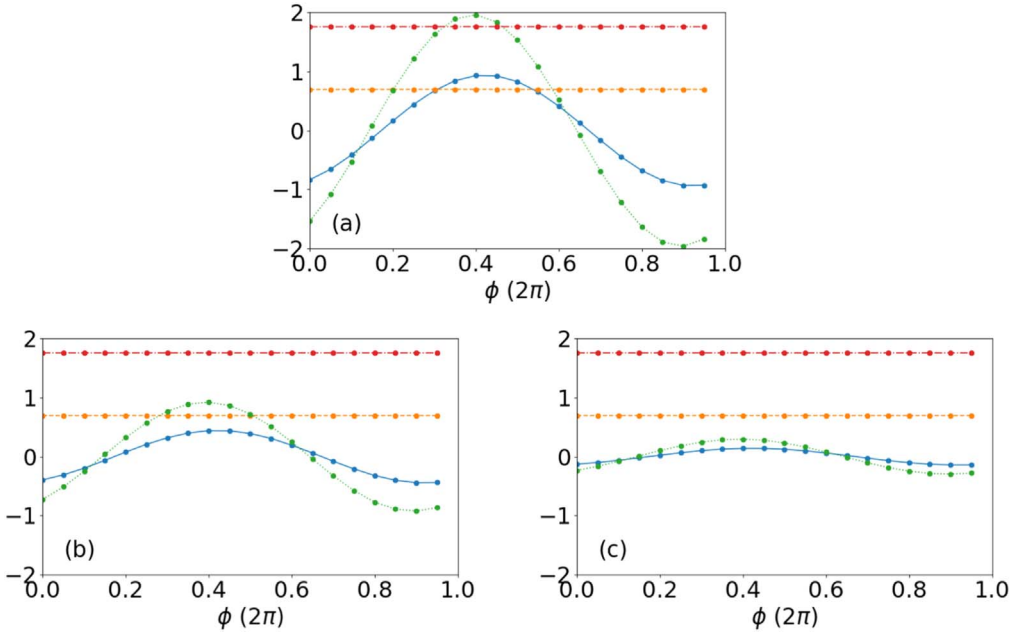

Figure 7. Anisotropy parameters β_1 (solid line), β_2 (dashed line), β_3 (dotted line) and β_4 (dashed–dotted line) as function of carrier-envelope-phase. The results averaged using a Gaussian distribution for the CEP (see, equation (6)) with widths of (b) $\alpha = 0.2$ (in units of 2π) and (c) $\alpha = 0.4$ are compared with the unaveraged results (a). Peak intensity: 10^{11} W cm^{-2}, central frequency: $\omega_0 = |E_{1s} - E_{2p}|$, pulse duration: 1.2 FWHM cycles and photoelectron energy $2\omega_0 - |E_{1s}|$.

pulse duration) is required for the same value of $f(\Omega)/f^2(\omega)$ than at photoelectron energies below $E = 2\omega_0 - I_p$ (dashed line), where $\omega < \omega_0$ while $\Omega > \omega_0$.

In the limit of short pulses and high intensities, both the one- and three-photon processes can interfere since the three-photon process scales with I^3. The results for the anisotropy parameter β_5 in figure 6 confirm this expectation. At a photoelectron energy of $2\omega_0 - |E_{1s}|$ (panel (a)) a peak intensity of about 10^{14} W cm^{-2} and a rather large spectral bandwidth is required to facilitate the three-photon process with significant probability since the corresponding photon energies are smaller than the central frequency. The distribution over photoelectron energy (panel (b)) shows that the impact of the three-photon ionization process is indeed more visible at energies near $E = 3\omega_0 - |E_{1s}|$.

3.3. Impact of pulse fluctuations

For the discussion in the previous subsection we have considered results obtained at fixed pulse parameters. The results in figures 4 and 5 show that the transition regime occurs over a rather small window of pulse duration while it appears to be rather stable for variations of the peak intensity up to half an order of magnitude. The photon energies in the extreme ultraviolet can be nowadays generated using high-order harmonics or free electron lasers. In view of the technical difficulties to control the CEP of ultrashort pulses as well as the fluctuating pulse shapes in the self-amplified spontaneous emission (SASE) mode of free electron lasers, we have studied the impact of these variations on the anisotropy parameters.

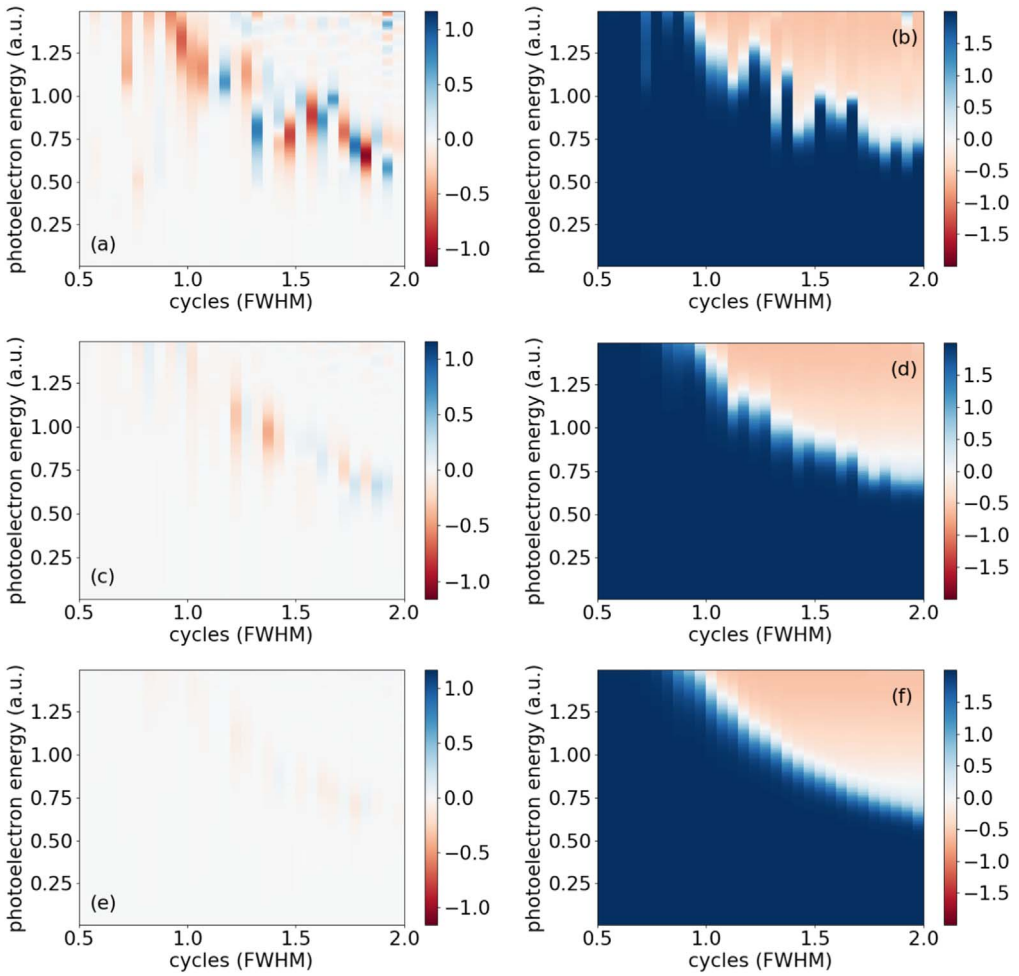

Figure 8. Anisotropy parameters β_1 (left) and β_2 (right) as function of pulse duration of the Gaussian window used in modeling the FEL pulses and photoelectron energy averaged over 10 (middle row) and 200 (bottom row) partially incoherent free electron pulses as compared to a single shot result (top row). Peak intensity of the Gaussian window: $I_0 = 10^{11}$ W cm^{-2} and central frequency of the spectral distribution $\omega_0 = |E_{1s} - E_{2p}|$.

To study the dependence on the CEP we have averaged the results about a given value ϕ_0 using a Gaussian distribution of width α as:

$$\beta_j^{(\alpha)}(\phi_0) = \frac{\sum_i \exp\left[-\frac{1}{2}\left(\frac{|\phi_i - \phi_0|}{2\pi\alpha}\right)\right]\sigma(\phi_i)\beta_j(\phi_i)}{\sum_i \exp\left[-\frac{1}{2}\left(\frac{|\phi_i - \phi_0|}{2\pi\alpha}\right)\right]\sigma(\phi_i)}, \quad (6)$$

where $\sigma(\phi_i)$ is the total ionization probability at CEP ϕ_i. The results for averages with (b) $\alpha = 0.2$ and (c) $\alpha = 0.4$ are compared in figure 7 with the unaveraged results (panel (a)). As expected, the odd β-parameters, which reflect the interference between the one- and two-photon processes, strongly depend on CEP, while the even parameters are independent of it. Thus, the transition from one-photon to two-photon ionization can be observed via β_2 and β_4 even in pulses without CEP stabilization. Although the odd parameters depend on CEP, the corresponding results appear to be indicative for the transition up to fluctuations of about $\pi/2$.

We have further studied the impact of fluctuations of temporal FEL laser pulse shapes [27]. We note that current FEL technology does not provide the bandwidth required to generate pulses down to the one- or two-cycle limit at the photon energies considered here. We may still attempt to give some theoretical insights concerning the robustness of the signal against the major fluctuations present in an FEL pulse. To this end, we have applied a partial coherence method, which has been used before to model longer FEL pulses [28]. We note that future technological progress towards generation of ultrashort FEL pulses in the EUV regime may necessitate to extent the current approach.

To generate the FEL pulses used in the numerical simulations, the spectrum of a vector potential with Gaussian envelope corresponding to peak intensity I_0 and FWHM pulse duration τ_0 is used as an input. Each spectral component is then multiplied with a random phase factor and an inverse Fourier transform is taken producing $A'(t)$, which is then normalized and windowed in time to give:

$$A_{\mathrm{FEL}}(t) = A_0 f(t) \frac{Re[A'(t)]}{\max|Re[A'(t)]|}, \quad (7)$$

where A_0 is given below equation (3) and $f(t)$ represents the envelope, here a Gaussian envelope. The electric field of the FEL pulse is then obtained using equation (4). The resulting pulse simulates the partially coherent nature of the SASE pulses produced by an FEL. The average of results from

numerical simulations over an increasing number of shots is expected to resemble results similar to those produced during an FEL beam-time. Here, the β-parameters are calculated using a weighted average

$$\beta_j^{\mathrm{FEL}}(E) = \frac{\sum_i^{N_{shots}} \sigma_i(E)\beta_{j,i}(E)}{\sum_i^{N_{shots}} \sigma_i(E)}, \tag{8}$$

to account for the photoelectron yield shot to shot.

In figure 8 we compare the results for β_1^{FEL} (left) and β_2^{FEL} (right) as function of photoelectron energy and pulse duration of the Gaussian window used in modeling the FEL pulses, averaged over 10 (panels (c), (d)) and 200 (panels (e), (f)) FEL shots for each pulse length (i.e. 6200 calculations in total) with the exemplary results from a single shot (panels (a), (b)). A robust distribution for β_2^{FEL} emerges as the number of shots increases, clearly showing the transition from a one- to a two-photon process (the same conclusion holds for β_4^{FEL}, not shown). However, the interference in the PADs cannot be determined via FEL laser pulses, since the results for β_1^{FEL} and β_3^{FEL} (not shown) average to zero in the transition regime. We note that the generated FEL pulses are not transform-limited and the pulse duration of the Gaussian window used in modeling the pulses does not correspond to that of Gaussian pulses used in the previous section 3.2. Comparing the data presented in figure 8(f) with those in figure 5(d) we estimate that the effective pulse duration of a bandwidth-limited Gaussian pulse with a spectrum corresponding to the average spectrum of the generated FEL pulses is about 0.6 times shorter than that of the Gaussian window.

4. Summary

In this work we have provided theoretical results, obtained from numerical solutions of the time-dependent Schrödinger equation, for the competition between one-photon and two-photon ionization in an ultrashort EUV laser pulse. We have shown that the transition between the two processes can be observed in the PADs and the related anisotropy parameters β_i ($i = 1, \ldots 4$) as function of pulse duration, peak intensity, central photon frequency and photoelectron energy distribution. While the even β-parameters exhibit the transition via a change from zero to a finite value, the odd parameters indicate the interference regime. At given photon and photoelectron energies this regime extends over about 0.5 FWHM cycles in duration and a variation by a factor of 2–5 in peak intensity. The impact of three-photon ionization, which becomes available at these broadband pulses as well, is seen at high intensities and large photoelectron energies. Finally, we have considered typical variations in the CEP of ultrashort pulses, e.g. as produced in HHG, and fluctuating pulse shapes in FEL pulses. It is found that the transition between one- and two-photon ionization can be observed via the even β-parameters in FEL pulses and pulses without CEP stabilization.

Acknowledgments

This work was primarily supported (JV, AB) by a grant from the US Department of Energy, Division of Chemical Sciences, Atomic, Molecular and Optical Sciences Program (Award No. DE-SC0001771). AJ-B acknowledges support by a grant from the US National Science Foundation (Grant No. PHY-1734006).

ORCID iDs

J Venzke https://orcid.org/0000-0003-4582-3388
A Jaroń-Becker https://orcid.org/0000-0003-2339-8544

References

[1] Nikolopoulos L A A and Lambropoulos P 2001 *J. Phys. B: At. Mol. Opt. Phys.* **34** 545
[2] van der Hart H W and Bingham P 2005 *J. Phys. B: At. Mol. Opt. Phys.* **38** 207
[3] Shakeshaft R 2007 *Phys. Rev.* A **76** 063405
[4] Pi L-W and Starace A F 2010 *Phys. Rev.* A **82** 053414
[5] Florescu V, Budriga O and Bachau H 2011 *Phys. Rev.* A **84** 033425
[6] Sato T *et al* 2011 *J. Phys. B: At. Mol. Opt. Phys.* **44** 161001
[7] Haber L H, Doughty B and Leone S R 2011 *Phys. Rev.* A **84** 013416
[8] Florescu V, Budriga O and Bachau H 2012 *Phys. Rev.* A **86** 033413
[9] Ishikawa K L and Ueda K 2012 *Phys. Rev. Lett.* **108** 033003
[10] Ishikawa K L and Ueda K 2013 *Appl. Sci.* **3** 189
[11] Ma R *et al* 2013 *J. Phys. B: At. Mol. Opt. Phys.* **46** 164018
[12] Rey H F and der Hart H W 2014 *J. Phys. B: At. Mol. Opt. Phys.* **47** 225601
[13] Grum-Grzhimailo A N, Gryzlova E V, Staroselskaya E I, Venzke J and Bartschat K 2015 *Phys. Rev.* A **91** 063418
[14] Douguet N, Grum-Grzhimailo A N, Gryzlova E V, Staroselskaya E I, Venzke J and Bartschat K 2016 *Phys. Rev.* A **93** 033402
[15] Hofbrucker J, Volotka A V and Fritzsche S 2017 *Phys. Rev.* A **96** 013409
[16] Hofbrucker J, Volotka A V and Fritzsche S 2018 *Phys. Rev. Lett.* **121** 053401
[17] Boll D I R, Fojon O A, McCurdy C W and Palacios A 2019 *Phys. Rev.* A **99** 023416
[18] Wang M-X, Liang H, Xiao X-R, Chen S-G and Peng L-Y 2019 *Phys. Rev.* A **99** 023407
[19] Kornilov O, Wang C C, Bünermann O, Healy A T, Leonard M, Peng C, Leone S R, Neumark D N and Gessner O 2010 *J. Phys. Chem.* A **114** 1437
[20] Rouzee A *et al* 2011 *Phys. Rev.* A **83** 031401(R)
[21] Ullrich J, Moshammer R, Dorn A, Dörner R, Schmidt L P H and Schmidt-Böcking H 2003 *Rep. Prog. Phys.* **66** 1463
[22] Venzke J, Reiff R, Xue Z, Jaroń-Becker A and Becker A 2018 *Phys. Rev.* A **98** 043434
[23] Scrinzi A 2010 *Phys. Rev.* A **81** 053845
[24] Chelkowski S and Bandrauk A D 2002 *Phys. Rev.* A **65** 061802
[25] Venzke J, Joyce T, Xue Z, Becker A and Jaroń-Becker A 2018 *Phys. Rev.* A **98** 063409
[26] Laplanche G, Jaouen M and Rachman A 1986 *J. Phys. B: At. Mol. Opt. Phys.* **19** 79
[27] Mitzner R *et al* 2008 *Opt. Express* **16** 19909
[28] Pfeiffer T, Jiang Y, Düsterer S, Moshammer R and Ullrich J 2010 *Opt. Lett.* **35** 3441